

A Sensitivity Study of the Effect of Horizontal Photon Transport on the Radiative Forcing of Contrails

AMANDA GOUNOU AND ROBIN J. HOGAN

Department of Meteorology, University of Reading, Reading, United Kingdom

(Manuscript received 10 April 2006, in final form 7 August 2006)

ABSTRACT

With the rapid growth in air travel, there is concern over the radiative impact of contrails and aircraft-induced cirrus on climate. Previous radiation calculations on contrails have almost all used the independent column approximation, which neglects the transport of photons through the sides of the contrail, but in this study the 3D effects are quantified using the Spherical Harmonic Discrete Ordinate Method (SHDOM). The authors have investigated the dependence of shortwave and longwave radiative forcing on contrail aspect ratio, optical depth, solar zenith angle, solar azimuth angle relative to contrail orientation, particle size, particle habit, surface albedo, and surface temperature. It is found that inclusion of 3D transport results in an increase in the positive longwave radiative forcing of the contrail and either an increase or a decrease in the magnitude of the negative shortwave radiative forcing depending on the orientation of the contrail with respect to the sun. Although these two effects are individually quite modest (of order 10%), the fact that the total shortwave and longwave forcings largely cancel during the day means that the relative change in the net radiative forcing due to the 3D effect is substantial; in some cases this results in a doubling of the net forcing of the contrail, in other cases changing its sign. On a more general note, the relatively simple geometry of contrail cirrus provides an ideal test case for explaining the various mechanisms by which 3D photon transport can change the radiative effect of clouds, which can be rather difficult to visualize for more complex cloud scenarios.

1. Introduction

A significant increase in air traffic in recent years has triggered concern about the impact of contrails on climate (Fahey et al. 1999). Contrails perturb the radiation budget of the earth by both reflecting incoming shortwave radiation back to space and enhancing the greenhouse effect in the longwave, the net effect being determined by the balance between the two. In previous studies based on the plane-parallel approximation (or independent column approximation; ICA), the longwave warming effect on climate (a positive radiative forcing) has been found to exceed the shortwave cooling effect (a negative radiative forcing) leading to a net warming effect (Meerkötter et al. 1999; Strauss et al. 1997). Nonetheless, the two effects are of similar magnitude, and uncertainties in forcing have been

found due to the various assumptions made, particularly regarding particle size, optical depth, and contrail cover. Fahey et al. (1999) estimate that the global mean net top-of-atmosphere radiative forcing of contrails is 0.02 W m^{-2} (with an uncertainty of a factor of 3 to 4), although this value is expected to increase by around a factor of 6 by 2050. The local forcing in the vicinity of major airports can be much larger (Stuber et al. 2006).

Three-dimensional radiative transfer calculations are more accurate than ICA calculations but are computationally expensive. The effect of 3D photon transport on the radiative forcing of clouds other than contrails has been studied in detail, and has been found to be particularly significant for shallow cumulus (e.g., Marshak and Davis 2005; Pincus et al. 2005). The only such study with contrails was that of Schulz (1998) who investigated the effect of horizontal photon transport on the albedo of a contrail simulated by a large-eddy model. He studied the sensitivity to solar zenith angle, but implicitly kept the solar azimuth angle fixed and parallel to the contrail (i.e., $\phi = 90^\circ$ in Fig. 1). The result was that for realistic contrail optical depths, the

Corresponding author address: Dr. Robin Hogan, Department of Meteorology, University of Reading, Earley Gate, P.O. Box 243, Reading, RG6 6BB, United Kingdom.
E-mail: r.j.hogan@reading.ac.uk

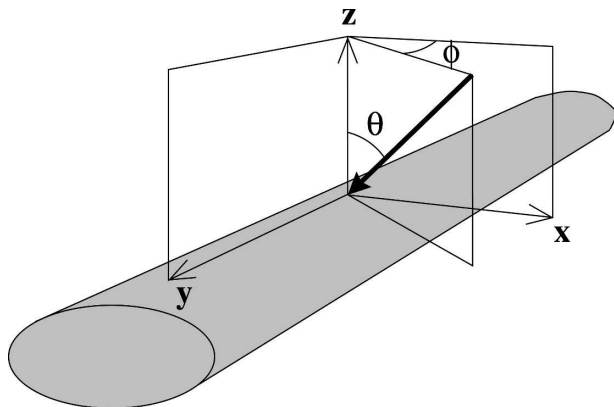


FIG. 1. Schematic showing the orientation of the contrail with respect to the direction of the sun (shown by the thick arrow), as described by the solar zenith angle (θ) and solar azimuth angle (ϕ). Also shown are orthogonal coordinate vectors x , y , and z , with the contrail aligned along the y axis.

3D transport caused only a slight reduction of the shortwave albedo at all solar zenith angles, compared to ICA.

In this study, the influence of horizontal photon transport on the radiative forcing of idealized contrails is investigated, in particular the dependence on solar zenith and azimuth angle, optical depth, contrail aspect ratio, the size and shape of the ice particles, surface albedo, and surface temperature. By considering both longwave and shortwave effects, we are able to investigate whether the relative size of the two effects is impacted in such a way as to change the net forcing. In section 2, the radiative transfer model used in this study is described, together with the experiments performed. In section 3, we present the effect of horizontal photon transport on contrail radiative forcing, and its sensitivity to the properties listed above.

2. Method

a. Radiative transfer model

The Spherical Harmonics Discrete Ordinates Method (SHDOM) was used in the radiative transfer calculations (Evans 1998). Spectral integration was performed using the correlated- k distribution method with the Rapid Radiative Transfer Model (RRTM) database of optical properties (Mlawer et al. 1997). The terrestrial spectral range was divided into 14 bands and the solar spectrum into 16 bands. The U.S. Standard Atmospheric profile (McClatchey et al. 1972) of temperature, pressure, water vapor, and ozone was used, which has a temperature of 288.1 K at the surface. In addition to water vapor and ozone, the radiation calculations

included fixed mixing ratios of carbon dioxide, methane and nitrous oxide. The water vapor continuum was included.

The idealized contrail was assumed to be infinite in length by using a 2D domain consisting of a slice through the contrail, with periodic boundary conditions in both horizontal directions. The calculations were performed using a 15-km wide and 50-km high domain with a spatial resolution of 100 m in the horizontal and 50 m in the vertical at contrail level and lower vertical resolution above and below the contrail. An angular resolution of 8 zenith angles and 16 azimuth angles was used. Tests on the influence of spatial and angular resolutions showed that the results had converged and hence a higher resolution was not needed. Tests also confirmed that a 15-km wide domain was sufficient to prevent significant interaction of photons between neighboring contrails through the periodic boundaries of the domain. Although contrails often occur in groups, to study horizontal photon interaction (e.g., via the shadowing of one contrail by another), one would need to use a fully 3D domain in order to represent contrails oriented at an arbitrary angle with respect to one another. This would greatly increase the computational cost so is beyond the scope of the present study, but basically the effect of interaction between two contrails would be to slightly reduce the radiative forcing compared to the sum of the forcings from two isolated contrails.

The contrail was 400-m thick, lying between altitudes of 9.8 and 10.2 km, and the temperature was 221.5 K at the top of the contrail; observations have shown these to be typical values (Sassen 1997). No other clouds were present in the domain. The surface shortwave albedo was set to 0.15 and the longwave emissivity to 0.98.

A feature of the SHDOM model is that, in addition to 3D calculations, 1D calculations can be performed using the independent column approximation. When this option is used, the model effectively considers each column as a separate, horizontally uniform domain of infinite horizontal extent, without allowing transfer of radiation from one column to another. This is what all previous published studies of contrails except that of Schulz (1998) have assumed.

b. Experiments performed

A control experiment was initially performed on what was intended to represent a typical contrail, followed by a number of sensitivity tests based on the range of contrail properties found in the literature. The control contrail was 400 m thick and 800 m wide with a mean optical depth of 0.2 at 0.55 μm (henceforth all

references to optical depth will be for this wavelength). An effective radius of 10 μm was taken for the size of the particles. The contrail was elliptical in cross section with an ice water content (IWC) dependence on horizontal distance x and vertical distance z given by

$$\text{IWC} = \begin{cases} \text{IWC}_p \cos\left(\frac{\pi}{2} r\right) & \text{for } r < 1; \\ 0 & \text{for } r \geq 1, \end{cases}$$

where

$$r = \left[\left(\frac{x - x_0}{\Delta x/2} \right)^2 + \left(\frac{z - z_0}{\Delta z/2} \right)^2 \right]^{1/2},$$

where Δx is the contrail width, Δz is the contrail thickness, x_0 and z_0 are the horizontal and vertical positions of the center of the contrail and IWC_p is the peak ice water content in the center of the contrail. The elliptical cross section is a rough approximation to contrails both observed by lidar (Freudenthaler et al. 1995; Sassen 1997) and modeled (Sassen 1997; Schulz 1998). The formula above results in peak concentrations toward the center of the contrail, in agreement with both lidar observations and model results showing extinction coefficient increasing toward the interior of the contrail. It should be noted that for the control contrail the photon mean free path at 0.55 μm is around 2 km, larger than the width of the contrail, and therefore the radiative properties will be insensitive to any small-scale inhomogeneities that may be present within the contrail.

The optical properties of solid columns (Yang et al. 2000) were used for the shortwave calculations. Scattering and extinction data were only available up to a wavelength of 4 μm so for the longwave computations we used optical properties of spheres calculated using Mie theory. From satellite observations, the mean optical depth of contrails has been estimated to be between 0.1 and 0.2 (Meyer et al. 2002), but larger optical depths of up to 0.6 have been measured by ground instrumentation (Sassen 1997). We show results for optical depths of 0.2 and 0.4.

The size of the ice particles mainly depends on the availability of water and the number of nuclei. According to previous in situ measurements (Strauss et al. 1997; Lawson et al. 1998; Liou et al. 1998) persistent contrails typically have an effective radius between 10 and 25 μm . However, in a more recent study using optical spectrometers and ice replicators, Schröder et al. (2000) estimated the mean effective radius to be smaller, about 5 μm . Therefore, in the experiments, the sensitivity of the radiative forcing with ice particle size was investigated through the range 5–25 μm .

As the ice particles remain small in contrails, their

shapes tend to be quite simple. Schröder et al. (2000) found that they were almost spherical, but solid columns and bullet rosettes have also been reported (Liou et al. 1998; Goodman et al. 1998) particularly in the periphery of the contrail (Lawson et al. 1998). The control experiment was carried out using the optical properties of solid columns but six-branched bullet rosettes and spheres were also tested.

The horizontal and vertical growth of a contrail depends on the ambient conditions. The vertical growth is limited by wind shear and temperature stratification. According to a lidar-based study by Freudenthaler et al. (1995), the thickness of a persisting contrail varies between 200 and 700 m, and its width from 500 m up to several kilometers. The thickness of the contrail was kept constant at 400 m in this study but the width was varied from 400 to 1200 m. To test the sensitivity to surface albedo and surface temperature, calculations were also performed for a high-latitude winter temperature profile over snow with a surface albedo of 0.8.

A range of solar zenith angles (θ) and two solar azimuth angles (ϕ) were tested, as illustrated in Fig. 1. Figure 2 illustrates the shortwave downwelling and longwave upwelling fluxes in the 2D domain, for a contrail illuminated from the side ($\theta = 50^\circ$ and $\phi = 0^\circ$). The periodic nature of the domain is illustrated in Fig. 2a, while Fig. 2b shows the reduction in upwelling longwave radiation above the cold contrail.

The radiative forcing (RF) was calculated by computing the difference between the horizontally averaged upwelling fluxes at the top of the domain (50-km altitude) in clear-sky conditions and when the contrail was present, such that a negative RF indicates a cooling effect on climate and a positive RF indicates a warming effect. For ease of comparison with other studies the RF is scaled up to the equivalent value for a 100% contrail cover, although it should be stressed that this is just a mathematical exercise as of course a homogeneous contrail with 100% contrail cover would not exhibit any 3D effect.

3. Results

a. Sensitivity to solar zenith and azimuth angle

Figure 3a shows the variation of longwave, shortwave, and net RF with solar zenith angle when the calculations are done with the ICA (solid line) and the 3D model (dashed and dotted lines). As shown by the two upper lines in Fig. 3a, the longwave RF does not of course vary with solar zenith angle as the temperature profile was kept constant. The 3D calculations (dotted line) give a constant value of 25.8 W m^{-2} for a 100% contrail cover whereas the ICA calculations (solid line)

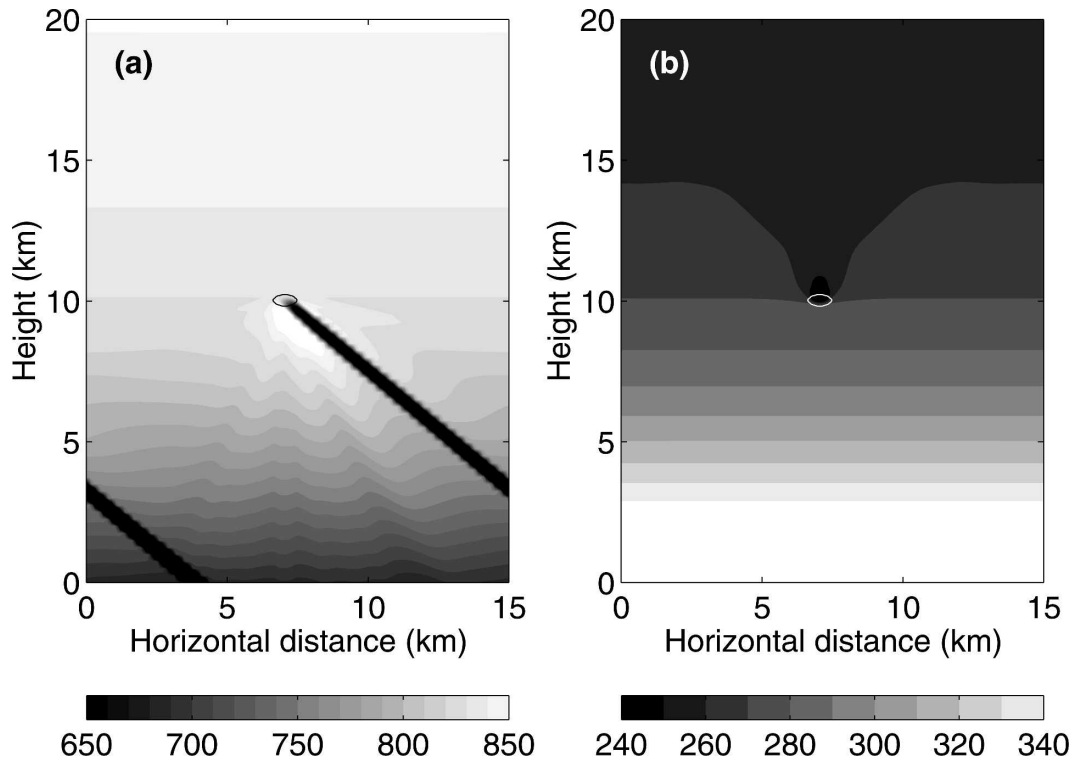


FIG. 2. (a) Shortwave downwelling flux and (b) longwave upwelling flux (in W m^{-2}) in the presence of a contrail, calculated using the 3D SHDOM model. The contrail is represented as an $800 \text{ m} \times 400 \text{ m}$ ice cloud with a mean optical depth of 0.4 at $0.55 \mu\text{m}$, composed of solid columns. The solar zenith angle was 50° and solar azimuth angle 0° . The black and white ellipses indicate the 1 mg m^{-3} ice water content contour.

show a longwave RF of 24.0 W m^{-2} . The horizontal photon transport thus increases the longwave RF by 1.8 W m^{-2} (or 7.5%).

The reason that clouds have a warming effect in the longwave is that they absorb upwelling photons from lower in the atmosphere and reemit at a lower black-body temperature, and Fig. 2b illustrates the associated reduction in the upwelling radiation above the contrail. The 3D enhancement of the forcing may be explained with reference to the idealized schematic in Fig. 4. In both the ICA and full 3D scenario, the fraction of upwelling photons at the height of the base of the contrail that enter the contrail through the base is equal to the contrail fractional coverage. However, in the 3D scenario, an additional fraction of photons enter the contrail through the sides and have a chance of being absorbed, thereby further reducing the outgoing longwave radiation at the top of the atmosphere.

We now consider the shortwave RF for the sun parallel to the contrail ($\phi = 90^\circ$ in Fig. 1), as shown by the lowest dotted line in Fig. 3a. At a solar zenith angle $\theta = 0^\circ$, the shortwave RF is -14.1 W m^{-2} and increases in magnitude with θ reaching a maximum negative value of -25.2 W m^{-2} at $\theta \approx 75^\circ$. A difference of 0.6 W m^{-2}

is found between the ICA and 3D calculations corresponding to a weakening of about 5% in the shortwave RF when horizontal photon transport is included, for all solar zenith angles. The reason for this is illustrated in Fig. 5. In the 3D calculation, photons that enter the contrail through the top and are forward scattered have a chance to escape through the side of the contrail, whereas in the ICA those photons would remain within the contrail and hence have a greater probability of being backscattered back to space. This increases the albedo of the contrail, but because it only significantly modifies the multiply scattered photons, its magnitude is quite weak for such a low optical depth. This result is consistent with the findings of Schulz (1998).

The lowest dashed line in Fig. 3a shows the shortwave RF for the sun perpendicular to the contrail ($\phi = 0^\circ$ in Fig. 1). The same behavior as when the sun is parallel to the contrail occurs for zenith angles from 0° to around 67° . Beyond 67° , the shortwave RF becomes more negative, reaching a maximum negative value of -29 W m^{-2} at a solar zenith angle of 82° . This strengthening occurs because as the solar zenith angle increases, the sun begins to illuminate the sides of the contrail as well as the top, or equivalently, that the width of the

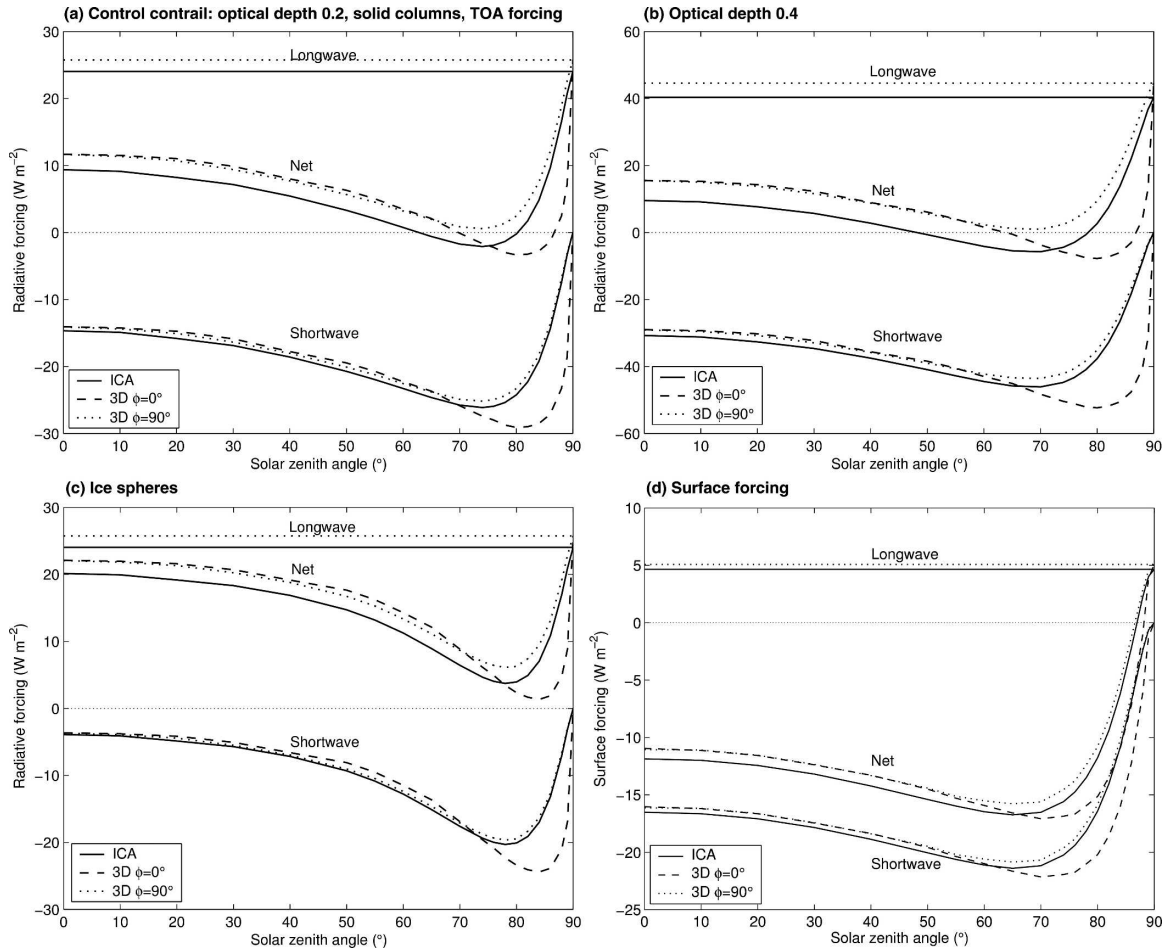


FIG. 3. (a) Shortwave, longwave, and net top-of-atmosphere (TOA) radiative forcing as a function of solar zenith angle for the independent column approximation (solid line), 3D radiative transfer with a solar azimuth angle of $\phi = 0^\circ$ corresponding to illumination of the contrail from the side (dashed line), and 3D radiative transfer with $\phi = 90^\circ$ corresponding to the sun in the same plane as the contrail (dotted line). The results have been scaled up to 100% contrail cover and are for a contrail with a mean optical depth of 0.2 at $0.55 \mu\text{m}$, an effective radius of $10 \mu\text{m}$, and composed of solid columns. (b) As in (a) but for a contrail with an optical depth of 0.4. (c) As in (a) but for a contrail composed of ice spheres. (d) As in (a) but for the surface radiative forcing rather than TOA forcing.

shadow cast by a contrail with width Δx increases above Δx as the solar zenith angle increases, as shown in Fig. 6. The resulting increase in the probability of an incoming photon intercepting a cloud and being scattered back to space results in an increase in the shortwave RF of the cloud compared to ICA. For intermediate values of solar azimuth angle ϕ , the shortwave RF lies between the curves shown for $\phi = 0^\circ$ and $\phi = 90^\circ$. It should be noted that the results are unreliable for solar zenith angles between 88° and 90° because of earth curvature effects.

The net radiative forcing is the sum of the positive longwave and negative shortwave effects, shown by the middle three lines in Fig. 3a. When the sun is parallel to the contrail, the longwave RF always dominates over the shortwave RF leading to a positive net RF of be-

tween 0.6 and 25.8 W m^{-2} . The horizontal photon transport increases the longwave RF and reduces the magnitude of the negative shortwave RF; that is, both processes lead to a warming effect. Separately these effects are quite small, but when we consider the net RF there can be an appreciable cancellation between the total longwave and shortwave effects resulting in the two small contributions adding up to give a quite significant contribution to the net RF. For $\theta \approx 40^\circ$, the net RF is almost doubled while at $\theta \approx 80^\circ$, it may be doubled or its sign reversed, depending on the azimuthal orientation of the sun relative to the contrail.

Figure 3d shows the surface forcing for the control contrail, defined as the effect of the contrail on the domain-mean surface downwelling-minus-upwelling ir-

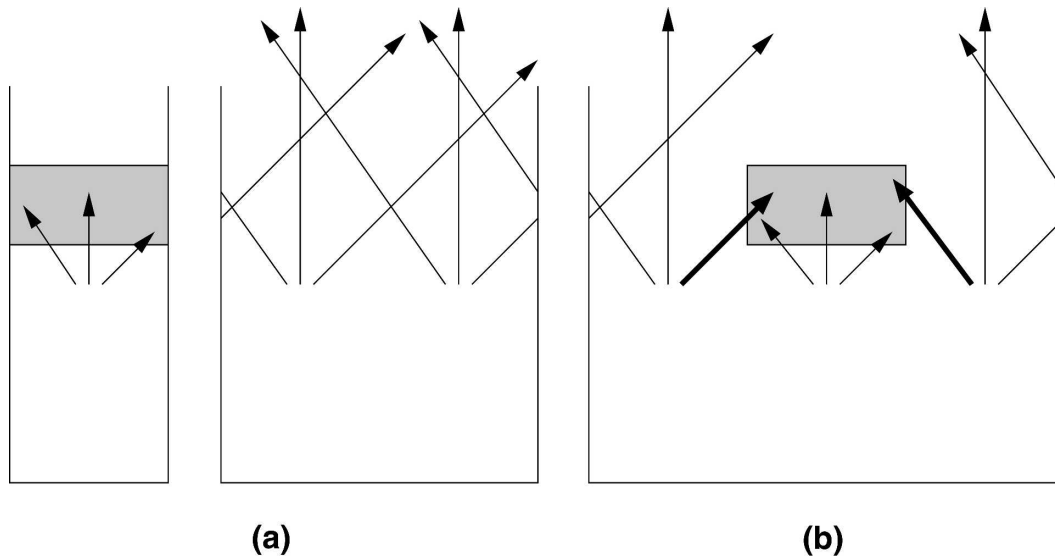


FIG. 4. Schematic illustrating the effect of 3D radiative transfer on longwave forcing. (a) The independent column approximation, in which the cloudy and clear-sky regions are treated separately in periodic domains such that the upwelling photons can only enter the cloud through its base. (b) The 3D radiative transfer case in which photons that would previously have escaped to space are able to enter the cloud through the sides (shown by the thick black arrows). If absorbed, the longwave TOA radiative forcing is thereby increased.

radiance, compared to clear sky. It can be seen that the longwave surface forcing is considerably smaller than the top-of-atmosphere forcing shown in Fig. 3a, because of absorption by water vapor in the lower troposphere leading to the closing of much of the infrared window (Fahey et al. 1999). Similarly, for $\theta > 80^\circ$, the

shortwave surface forcing is reduced compared to the top-of-atmosphere value due to the increased absorption associated with the longer pathlength through the atmosphere. In relative terms, the 3D effect in the shortwave and longwave is rather similar to its effect at top-of-atmosphere, but because of the much lower

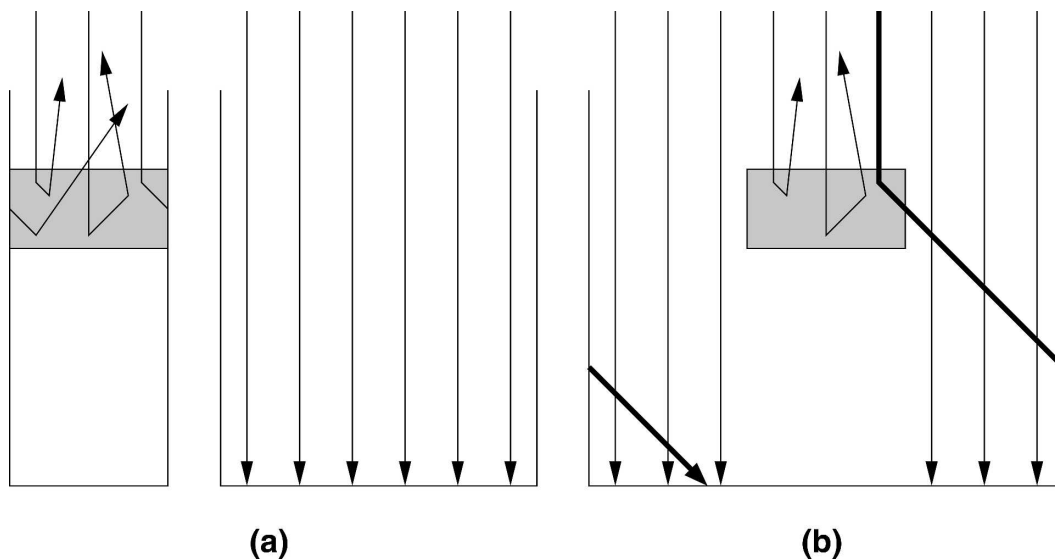


FIG. 5. Schematic of the shortwave radiation field in (a) the ICA model and (b) 3D model. In the 3D model, photons can travel horizontally and hence have more chance of reaching the surface highlighted by the thick black arrow. Thus, the shortwave radiative forcing is reduced. Note that this mechanism is only dominant when the sun does not illuminate the sides of the contrail, i.e., for low solar zenith angles or for a solar azimuth angle ϕ of 90° .

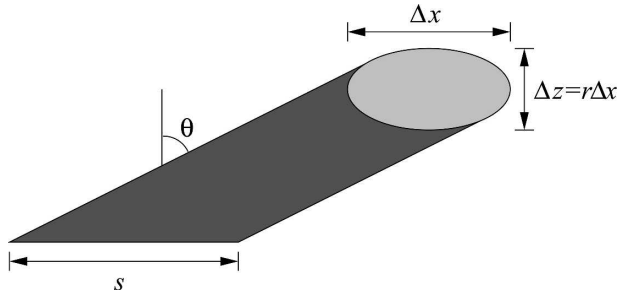


FIG. 6. Schematic demonstrating the shadow effect: a contrail of width Δx and aspect ratio r is illuminated by the sun with a solar zenith angle of θ and azimuth angle of $\phi = 0^\circ$ (see Fig. 1). If the contrail has an elliptical cross section then it can be shown that the width of the shadow cast s is greater than Δx , being given by $s = \Delta x(1 + r^2 \tan^2 \theta)^{1/2}$. Thus, for large θ , a greater fraction of incident photons will intercept the contrail than in the independent column approximation, resulting in a greater shortwave radiative forcing.

longwave effect at the surface, the relative effect of 3D transport on net forcing is much less at the surface.

b. Sensitivity to optical depth

Figure 3b shows the dependence of radiative forcing on solar zenith angle for a contrail with an optical depth of 0.4, which is twice the optical depth of the control contrail. We first consider the case when the sun is parallel to the contrail ($\phi = 90^\circ$), shown by the lowest dotted lines in Fig. 3b. Comparing Figs. 3a and 3b we can see that, at low solar zenith angles, the shortwave RF is approximately doubled when doubling the optical depth. However, at high solar zenith angles, the shortwave RF is less than twice the value for an optical depth of 0.2. Saturation occurs because of a large increase in photon pathlength through the contrail. In this case, the pathlength is inversely proportional to the cosine of zenith angle, because the photons travel similarly to how they would in an infinitely long contrail. The pathlength through the contrail in the ICA model is the same as in the 3D model for $\phi = 90^\circ$ and therefore saturation also occurs at high solar zenith angles. The 3D effect due to the mechanism shown in Fig. 5 is approximately proportional to the magnitude of shortwave radiative forcing, decreasing it by 5%, or around 1.8 W m^{-2} .

We consider now the sun perpendicular to the contrail ($\phi = 0^\circ$) as shown by the lowest dashed line in Fig. 3b. The saturation at high solar zenith angles does not occur in the same way as for $\phi = 90^\circ$, because the photon pathlength through a contrail illuminated from the side does not increase as much. However, the shadow effect is still just as important. Therefore, the effect of horizontal photon transport at high solar ze-

nith angles becomes larger when the optical depth is increased. At a solar zenith angle of 80° , the shortwave 3D effect enhances the total shortwave RF by 14.6 W m^{-2} , or around 40%.

The longwave RF in Fig. 3b is 44.6 W m^{-2} . Unlike the shortwave RF, it has not doubled compared to the calculations for an optical depth of 0.2, because as the optical depth increases the contrail tends toward a blackbody and the effect saturates. However, the longwave 3D effect is 4.3 W m^{-2} corresponding to a 10% increase; this is more than the 7.5% increase for an optical depth of 0.2. Likewise, for a contrail optical depth of 0.6, the percentage 3D effect increases to 12.2% (not shown).

The longwave RF saturates more rapidly than the shortwave RF but it increases in magnitude more than the shortwave RF (even if the percentage increase in longwave RF is smaller than the shortwave). Therefore, the net RF is slightly larger for an optical depth of 0.4 than for an optical depth of 0.2.

c. Sensitivity to ice particle size and shape

Figure 3c shows the variation of radiative forcing with solar zenith angle for a contrail formed with spherical ice particles. As can be seen by comparing the lowest lines in Figs. 3a and 3c, the shortwave RF has a stronger diurnal variation than when the contrail is formed with solid columns. At low solar zenith angles, the shortwave RF is smaller than for solid columns by about 80%. However, at high solar zenith angles, the shortwave radiative forcing is only 20% smaller than for solid columns. The reason is that spherical ice particles have a larger asymmetry factor g (e.g., at a wavelength of $0.55 \mu\text{m}$ and effective radius of $10 \mu\text{m}$, $g = 0.85$ for spheres compared to $g = 0.75$ for solid columns), which leads to more forward scattering and hence a much smaller shortwave radiative effect at low solar zenith angles. The effect of horizontal photon transport is approximately proportional to the shortwave RF, and therefore the magnitude of the effect is smaller than for solid columns. The calculations were done also for bullet rosettes but it was found that the results were very similar to those for solid columns.

As the longwave calculations were performed using Mie theory, the longwave RF calculation gave the same value as previously. The magnitude of the longwave RF for spheres is found to be always greater than the magnitude of the shortwave RF leading to the net RF always being positive.

Figures 7a and 7b show the sensitivity of RF to particle size at a solar zenith angle of 40° and 80° respectively. The mean optical depth at $0.55 \mu\text{m}$ was kept constant at 0.2 by varying the ice water content in ap-

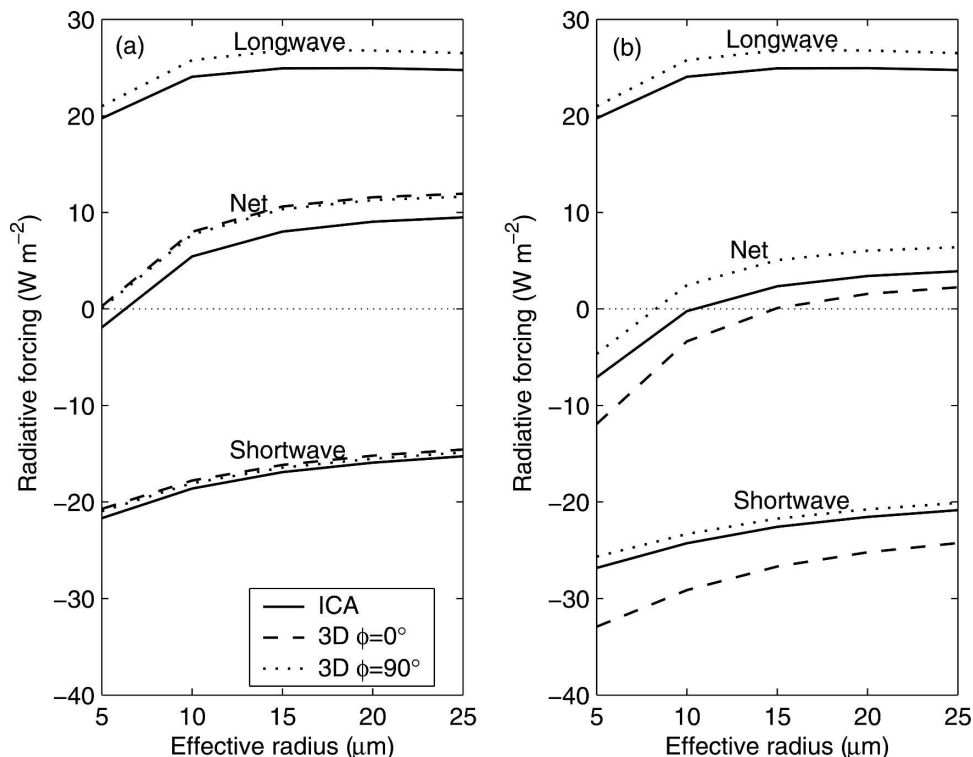


FIG. 7. Shortwave, longwave, and net TOA radiative forcings vs ice particle effective radius for a solar zenith angle of 40° and (b) 80° . The mean $0.55\text{-}\mu\text{m}$ optical depth of the contrail was kept constant at 0.2. All other properties are as for the control contrail. Radiative forcing has been scaled to the equivalent for 100% contrail cover.

proximate proportion to the effective radius. As shown by the lowest lines in Figs. 7a and 7b, there is a 20%–30% decrease in shortwave RF when the size of the particles increases from 5 to 25 μm . This is because the asymmetry factor increases with increasing effective radius, particularly at visible wavelengths where it increases from 0.71 for solid columns with an effective radius of 5 μm to 0.88 for an effective radius of 25 μm . There are thus more photons scattered in the forward direction and therefore the shortwave radiative forcing is smaller for larger particles.

The upper lines in Figs. 7a and 7b show the sensitivity of longwave RF to effective radius. As the size of the particles increases from 5 to 10 μm , there is a 25% increase in longwave RF but between 10 and 25 μm it is approximately constant. This is because when the particles are larger than the wavelength, the extinction efficiency tends toward an asymptotic value of 2, whereas smaller particles have a lower extinction efficiency.

As effective radius is increased, the longwave RF increases whereas the magnitude of the negative shortwave RF decreases, so the net RF due to contrails increases quite significantly. It changes from 0.3 to 11.9

W m^{-2} over the range 5–25 μm at a solar zenith angle of 40° and from -11.9 to 2.2 W m^{-2} for a zenith angle of 80° as shown by the middle dashed lines in Figs. 7a and 7b.

d. Sensitivity to contrail aspect ratio

Figures 8a and 8b show the variation of radiative forcing with contrail aspect ratio, again scaled to always be equivalent to 100% contrail cover. As can be seen from the upper lines in Fig. 8, while the ICA calculation shows a longwave RF constant with increasing contrail width, the 3D model predicts a decrease in longwave RF with increasing contrail width. The effect of horizontal photon transport is 3 times less when the width of the contrail is tripled, decreasing from 3 W m^{-2} for a $400 \times 400 \text{ m}$ contrail to 1 W m^{-2} for a $1200 \times 400 \text{ m}$ contrail. This is because the magnitude of the effect as shown in Fig. 4 increases in proportion of the area of contrail side. The shortwave effect is smaller when the contrail is wider but this is not directly proportional to the width, which suggests that the horizontal photon transport is also important within the contrail, between different extinction values.

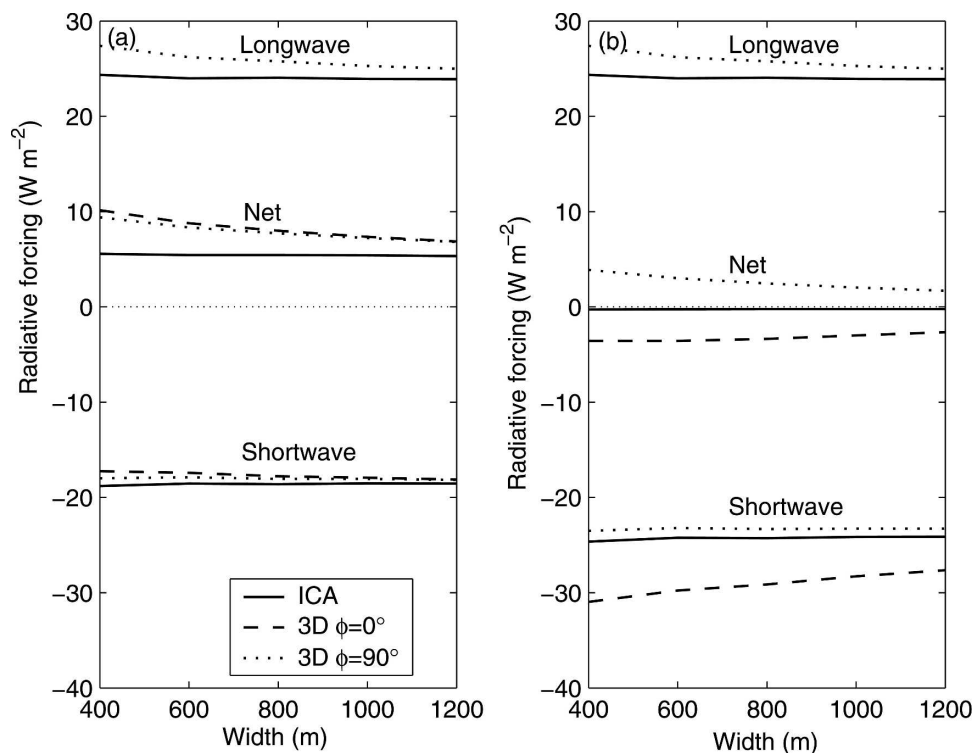


FIG. 8. Shortwave, longwave, and net TOA radiative forcings vs the width of the contrail for a solar zenith angle of (a) 40° and (b) 80° . All other properties are as for the control contrail. Radiative forcing has been scaled to the equivalent for 100% contrail cover.

e. Sensitivity to surface albedo and surface temperature

The sensitivity of contrail shortwave radiative forcing to surface albedo was studied by Myhre and Stordal (2001), who found a significant reduction in forcing as surface albedo was increased (or, equivalently, for contrails overlying low cloud). To investigate the sensitivity of the 3D effect to surface albedo and surface temperature, Fig. 9 shows the results of calculations performed to simulate a contrail over snow, by using a surface shortwave albedo of 0.8 and a longwave emissivity of 1.0. The control contrail was used, but was embedded in the sub-arctic winter standard atmosphere (McClatchey et al. 1972), which has a surface temperature of 257.1 K and a temperature at the top of the contrail of 217.2 K.

The longwave RF exhibits a reduction compared to the U.S. Standard Atmosphere (Fig. 3a), in approximate proportion to the reduction in the temperature difference between the ground and the contrail (from 66.6 to 39.9 K). However, the fractional increase in longwave RF when 3D transport is included is still 7.5%, indicating that the dominant factors controlling 3D effects in the longwave are optical depth and contrail aspect ratio.

The shortwave RF exhibits a large reduction in magnitude compared to that for a surface albedo of 0.15 (Fig. 3c) due to the decreased contrast in reflectance between contrail and clear sky when viewed from

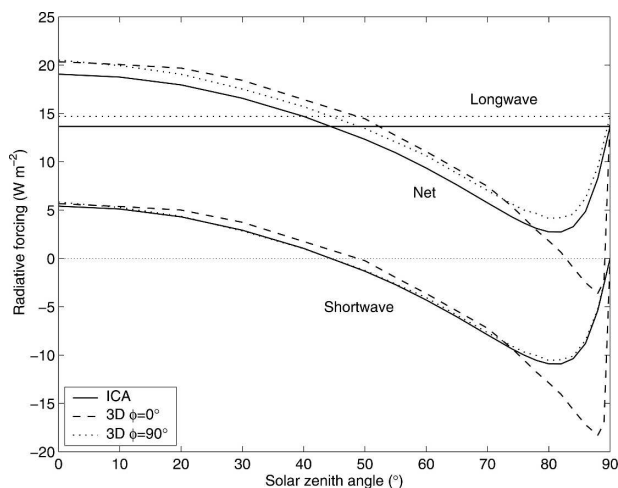


FIG. 9. Shortwave, longwave, and net TOA radiative forcing as a function of solar zenith angle, for the control contrail in the subarctic winter standard atmosphere over snow with a shortwave albedo of 0.8 and a surface temperature of -16.1°C . Radiative forcing has been scaled to the equivalent for 100% contrail cover.

above. A similar decrease would occur for the case of a contrail overlying an optically thick cloud. For the sun aligned parallel to the contrail ($\phi = 90^\circ$), the 3D effect is still small, less than 5%. For the sun aligned perpendicular to the contrail ($\phi = 0^\circ$) and large solar zenith angles ($\theta > 75^\circ$), the 3D effect is again very large, which feeds through to the net forcing. This is particularly important for radiative forcing calculations in the daytime arctic where the sun is usually not far above the horizon.

4. Conclusions

Almost all previous studies on contrail radiative forcing have neglected horizontal photon transport but in this paper, the 3D effect has been investigated for idealized contrails. The horizontal photon transport increases the longwave RF of contrails by around 10% because more photons can enter the cloud by the sides and so have more chance to be absorbed. The shortwave effect is strongly dependent on the orientation of the contrail with respect to the sun. When the sun is parallel to the contrail, the horizontal photon transport weakly decreases the magnitude of the RF by around 5% at all solar zenith angles. This is because in the 3D model, scattered photons can escape the contrail from the sides, which cannot happen in the ICA model. Conversely, when the sun is perpendicular to the contrail, the shadow effect strongly increases the shortwave RF at high solar zenith angles. For solar zenith angles less than around 70° , however, the horizontal photon transport decreases the magnitude of the negative shortwave RF and increases the positive longwave RF, which means that the two effects tend to increase the net RF, leading to warming tendency. Therefore, even if the individual contributions are small, when we consider the net RF, which is a subtle balance between the two, the effect of the horizontal photon transport becomes important.

The magnitude of the 3D effect increases with contrail optical depth, and it is found that the effect on the shortwave RF increases proportionally with increasing optical depth (i.e., the percentage effect remains the same) whereas the percentage effect on the longwave RF becomes larger when the optical depth increases. The aspect ratio of the contrail is also important, with the 3D effect being stronger for young contrails with an aspect ratio close to one but weakening for older contrails that tend to spread out preferentially in the horizontal direction. The significant effect of horizontal photon transport found in this paper suggests that there is a need to reevaluate the global impact of contrails on

climate to account for this effect. Clearly the SHDOM code is too slow to be run globally, but the simple shapes of the curves in Fig. 3 suggest that it should be possible to parameterize the 3D effect and apply it to global calculations performed using an ICA code.

Acknowledgments. We thank Keith Shine for valuable comments on the original manuscript, and Frank Evans for the use of the SHDOM code.

REFERENCES

- Evans, K. F., 1998: The spherical harmonics discrete ordinate method for three-dimensional atmospheric radiative transfer. *J. Atmos. Sci.*, **55**, 429–466.
- Fahey, D. W., and Coauthors, 1999: Aviation-produced aerosol and cloudiness. *Aviation and the Global Atmosphere, IPCC Special Report*, J. E. Penner et al., Eds., Cambridge University Press, 65–120.
- Freudenthaler, V., F. Homburg, and H. Jäger, 1995: Contrail observations by ground-based scanning lidar: Cross-sectional growth. *Geophys. Res. Lett.*, **22**, 3501–3504.
- Goodman, J., R. F. Pueschel, E. J. Jensen, S. Verma, G. V. Ferry, S. D. Howard, S. A. Kinne, and D. Baumgardner, 1998: Shape and size of contrails ice particles. *Geophys. Res. Lett.*, **25**, 1327–1330.
- Lawson, R. P., A. J. Heymsfield, S. M. Aulenbach, and T. L. Jensen, 1998: Shapes, sizes and light scattering properties of ice crystals in cirrus and a persistent contrail during SUCCESS. *Geophys. Res. Lett.*, **25**, 1331–1334.
- Liou, K. N., P. Yang, Y. Takano, K. Sassen, T. Charlock, and W. Arnott, 1998: On the radiative properties of contrail cirrus. *Geophys. Res. Lett.*, **25**, 1161–1164.
- Marshak, A., and A. B. Davis, 2005: *3D Radiative Transfer in Cloudy Atmospheres*. Springer, 686 pp.
- McClatchey, R. A., R. A. Fenn, J. E. A. Selby, P. E. Voltz, and J. S. Garing, 1972: Optical properties of the atmosphere. AFCRL Environmental Research Paper 411, Air Force Cambridge Research Laboratories, Bedford, MA, 113 pp. [Available from Air Force Research Laboratories, L. G. Hanscom Field, Bedford, MA 01730.]
- Meerkötter, R., U. Schumann, D. R. Doelling, P. Minnis, T. Nakajima, and Y. Tsushima, 1999: Radiative forcing by contrails. *Ann. Geophys.*, **17**, 1080–1094.
- Meyer, R., H. Mannstein, R. Meerkötter, U. Schumann, and P. Wendling, 2002: Regional radiative forcing by line-shaped contrails derived from satellite data. *J. Geophys. Res.*, **107**, 4104, doi:10.1029/2001JD000426.
- Mlawer, E. J., S. J. Taubman, P. D. Brown, M. J. Iacono, and S. A. Clough, 1997: Radiative transfer for inhomogeneous atmosphere: RRTM, a validated correlated-k model for the long wave. *J. Geophys. Res.*, **102**, 16 663–16 682.
- Myhre, G., and F. Stordal, 2001: On the tradeoff of the solar and thermal infrared radiative impact of contrails. *Geophys. Res. Lett.*, **28**, 3119–3122.
- Pincus, R., C. Hannay, and K. F. Evans, 2005: The accuracy of

- determining three-dimensional radiative transfer effects in cumulus clouds using ground-based profiling instruments. *J. Atmos. Sci.*, **62**, 2284–2293.
- Sassen, K., 1997: Contrail-cirrus and their potential for regional climate change. *Bull. Amer. Meteor. Soc.*, **78**, 1885–1903.
- Schröder, F., and Coauthors, 2000: On the transition of contrails into cirrus clouds. *J. Atmos. Sci.*, **57**, 464–480.
- Schulz, J., 1998: On the effect of cloud inhomogeneity on area average radiative properties of contrails. *Geophys. Res. Lett.*, **25**, 1427–1430.
- Strauss, B., R. Meerkötter, B. Wissinger, P. Wendling, and M. Hess, 1997: On the regional impact of contrails: Microphysical and radiative properties of contrails and natural cirrus clouds. *Ann. Geophys.*, **15**, 1457–1467.
- Stuber, N., P. M. Forster, G. Rädcl, and K. P. Shine, 2006: The importance of the diurnal and annual cycle of air traffic for contrail radiative forcing. *Nature*, **441**, 864–867.
- Yang, P., K. N. Liou, K. Wyser, and D. Mitchell, 2000: Parameterisation of the scattering and absorption properties of individual ice crystals. *J. Geophys. Res.*, **105**, 4699–4718.